Electrostatic coupling of ion pumps

J. Nieto-Frausto, P. Läuger,† and H.-J. Apell
Department of Biology, University of Konstanz, D-7750, Germany

ABSTRACT In this paper the electrostatic interactions between membrane-embedded ion-pumps and their consequences for the kinetics of pump-mediated transport processes have been examined. We show that the time course of an intrinsically monomolecular transport reaction can become distinctly nonexponential, if the reaction is associated with charge translocation and takes place in an aggregate of pump molecules. First we consider the electrostatic coupling of a single dimer of ion-pumps embedded in the membrane. Then we apply the treatment to the kinetic analysis of light-driven proton transport by bacteriorhodopsin which forms two-dimensional hexagonal lattices. Finally, for the case of nonordered molecules, we also consider a model in which the pumps are randomly distributed over the nodes of a lattice. Here the average distance is equal to that deduced experimentally and the elemental size of the lattice is the effective diameter of one single pump. This latter model is applied to an aggregate of membrane-embedded Na, K- and Ca-pumps. In all these cases the electrostatic potential considered is the exact solution calculated from the method of electrical images for a plane membrane of finite thickness immersed in an infinite aqueous solution environment. The distributions of charges (ions or charged binding sites) are considered homogeneous or discrete in the membrane and/or in the external solution. In the case of discrete distributions we compare the results from a mean field approximation and a stochastic simulation.

INTRODUCTION

Ion pumps are transmembrane proteins engaged in primary active transport of ions. Well known examples are the light-driven proton pump of halobacteria (bacteriorhodopsin), or the P-type ATPases of animal cells, such as the Na, K-pump or Ca-pump. An interesting feature of many ion pumps is their tendency to aggregate in the membrane. A prominent example is bacteriorhodopsin, which forms two-dimensional hexagonal lattices in the plasma membrane of Halobacterium halobium (Stoeckenius and Bogomolni, 1982). Other ion pumps, such as the Ca-ATPase or the Na,K-ATPase are thought to be present in the membrane as dimers or small oligomers (Nørby, 1987; Møller et al., 1982). When Na,K-ATPase is prepared from mammalian kidney, flat membrane fragments are obtained containing the pump protein in high density, up to 10^4 dimeric units per μm^2, corresponding to an average distance between the dimers of ≈ 10 nm (Deguchi et al., 1977; Zampighi et al., 1986). Similar high densities of pump proteins are found in membranous preparations of Ca-ATPase from sarcoplasmic reticulum (Taylor et al., 1984) or of H,K-ATPase from gastric mucosa (Rabon and Reuben, 1990).

Pump-mediated ion transport is thought to involve a cyclic sequence of conformational transitions and ion binding and release steps. In virtually all ion pumps studied so far, at least one of the reaction steps in the cycle is electrogenic, i.e., associated with translocation of electric charge. In the Na,K-ATPase, phosphorylation of the protein by ATP leads to occlusion of three cytoplasmic Na^+ ions, which are subsequently released to the extracellular medium. Recent studies using electrochromic dyes have shown that Na^+ release leads to large changes of electric field strength in the membrane in the vicinity of the pump protein (Bühler et al., 1991; Stürmer et al., 1991). A likely explanation for this change of local field strength consists in the assumption that the Na^+ ions are released from a binding pocket buried inside the pump protein. The variation of electrostatic potential associated with uptake or release of ions may affect an electrogenic process in a neighboring protein. Thus, in a dimer of independent pumps, the rate constant of ion release from one monomer should depend on whether release has already occured in the other monomer. Similarly, in a two-dimensional aggregate of pump molecules, such as the purple membrane of halobacteria, the rate constant of a charge-translocating reaction in a given pump protein may be expected to be a function of the charge state of the rest of the ensemble.

†Deceased 13 September 1990.
J. Nieto-Frausto's permanent address is Departmento de Física, Centro de Investigación y de Estudios Avanzados del Instituto Politecnico Nacional. Apdo Postal 14-740, México 07000 D.F.

0006-3495/92/01/83/13 $2.00

In this study we examine electrostatic interactions between membrane-embedded ion pumps and their consequences for the kinetics of pump-mediated transport processes. We show that the time course of an intrinsically monomolecular transport reaction can become distinctly nonexponential if the reaction is associated with charge translocation and takes place in an aggregate of pump molecules. The treatment given here can be applied to the kinetic analysis of light-driven proton transport by bacteriorhodopsin.

Bacteriorhodopsin is often investigated by relaxation experiments, where the proton is bound to the Schiff base in the center of the protein and released upon a light flash to the extracellular medium. The following binding of a proton from the cytoplasmatic interface is so slow that it does not interfere with the process of interest. Similar conditions hold for charge transition detecting experiments with Na,K-ATPase and Ca-ATPase, when induced by the ATP concentration jump method (Läuger, 1991).

Charge–charge interactions in aggregates of pump proteins

Electrostatic coupling in a dimer

We first consider the comparatively simple case of a dimer consisting of two identical pump molecules P1 and P2 (Fig. 1). The dimer is embedded in a lipid membrane separating two semi-infinite aqueous phases. The dielectric properties of the membrane are described by an average dielectric constant ϵ_m. Recent estimates of the effective dielectric constant of folded proteins range between 2.5 and 4 (Gilson and Honig, 1986). With a dielectric constant of 2 for the hydrocarbon core of the lipid, a value of $\epsilon_m = 3$ may thus be assumed a reasonable estimate for the average dielectric constant of the membrane.

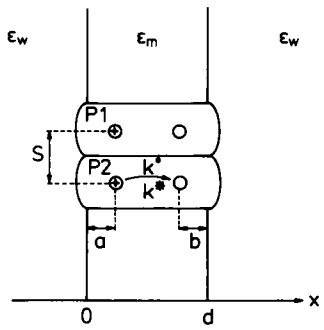

FIGURE 1 Pair of identical pump proteins, P1 and P2, embedded in a lipid membrane of average dielectric constant ϵ_m. The membrane separates two semi-infinite aqueous phases (dielectric constant ϵ_w). In each protein a transition can take place in which a charge Ze_0 is translocated from $x = a$ to $x = d - b$. Z is the valency and e_0 the elementary charge. k^0 and k^* are the rate constants of the transition under the condition that the neighboring charge is still in position $x = a$, or has moved to position $x = d - b$, respectively.

In each monomer, a transition can take place in which a charge Ze_0 moves from $x = a$ to $x = d - b$ (Fig. 1). Z is the valency, e_0 the elementary charge, and d is the membrane thickness. The rate constant of this transition obviously depends on whether in the other monomer a transition has already occurred. In the following, we denote by k^0 and k^* the rate constants under the condition that the neighboring charge is still in position $x = a$ (state E^0), or has moved to position $x = d - b$ (state E^*), respectively. k^0 and k^* depend on the electric potentials, $\Psi(a)$ and $\Psi(d - b)$, at points $x = a$ and $x = d - b$. If $\Psi^0(x)$ and $\Psi^*(x)$ are the potentials in states E^0 and E^*, respectively, k^0 and k^* may be expressed by the rate-theory equations:

$$k^0 = k_i \exp\left[Ze_0 \frac{\Psi^0(a) - \Psi^0(d-b)}{2k_BT}\right] \quad (1)$$

$$k^* = k_i \exp\left[Ze_0 \frac{\Psi^*(a) - \Psi^*(d-b)}{2k_BT}\right]. \quad (2)$$

k_i is the (hypothetical) intrinsic rate constant which would be present in the absence of this potential difference between $x = a$ and $x = d - b$. k_B is the Boltzmann's constant, and T the absolute temperature. Implicit in Eqs. 1 and 2 is the assumption that the activation barrier corresponding to the transition between states E^0 and E^* is symmetrical (Läuger, 1984).

Because dielectric boundaries exist at $x = 0$ and $x = d$, the field around the membrane-embedded charges is modified by the contribution of the induced electric polarization. For a given position of the charge Ze_0 in the protein P1, the potential $\Psi(x)$ along the x-axis can be calculated by the method of electrical images (Neumcke and Läuger, 1969; Flewelling and Hubbel, 1986; Honig et al., 1986). Introducing the relative difference θ between the dielectric constants:

$$\theta = \frac{\epsilon_w - \epsilon_m}{\epsilon_w + \epsilon_m}, \quad (3)$$

the potential $\Psi(x)$ inside protein P2 due to the charge in P1 is obtained as

$$\Psi(x) = \frac{Ze_0}{4\pi\epsilon_0\epsilon_m}\left[-\sum_{n=0}^{\infty}\frac{\theta^{2n+1}}{\sqrt{s^2 + (x + a + 2nd)^2}} + \sum_{n=0}^{\infty}\frac{\theta^{2n}}{\sqrt{s^2 + (x - a + 2nd)^2}} + \sum_{n=1}^{\infty}\frac{\theta^{2n}}{\sqrt{s^2 + (x - a - 2nd)^2}} - \sum_{n=1}^{\infty}\frac{\theta^{2n-1}}{\sqrt{s^2 + (x + a - 2nd)^2}}\right], \quad (4)$$

where $\epsilon_0 = 8.85 \cdot 10^{-12}\, CV^{-1}m^{-1}$ is the permitivity of free space, s is the distance between monomers in a dimer, and $0 \leq x \leq d$, (Fig. 1).

In the model represented in Fig. 1, it is assumed that each monomer bears a net charge $Ze_0 > 0$. This means that negative counter charges exist in the aqueous media which electrically neutralize the charge Ze_0 and which may influence the potential $\Psi(x)$. The distribution of the counter charges on the aqueous side of the membrane-solution interface depends on the ionic strength of the solution. In the following we assume that the ionic strength is high enough so that the counter charges are located in the interface. The limit of large ionic strength corresponds to a highly conductive aqueous medium, which is characterized by a large dielectric constant ($\epsilon_w \gg \epsilon_m$). Accordingly, for a preliminary calculation of $\Psi(x)$, effects of counter charges on $\Psi(x)$ are neglected.

By calculating $\Psi(x)$ from Eq. 4, the ratio k^0/k^* of the transition rate constants can be evaluated as a function of the parameters of the model. The results shown in Fig. 2 were obtained assuming the values $\epsilon_w = 80$, $Z = 1$, $k_BT/e_0 = 25$ mV, $a = 3$ nm, $d = 6$ nm, and $b = 0$, which corresponds to complete release of a univalent cation from a binding site located in the middle of the membrane. In Fig. 2 *a* the fast convergence of the series in Eq. 4 is shown. It can be seen that the terms with $n > 10$ no longer contribute significantly to the results of the calculations. To reduce numerical uncertainties as far as possible in corresponding calculations the summations have been performed up to 100 terms. Fig. 2 *b* shows the influence of the dielectric constant of the membrane and the distance, s, between the two pumps.

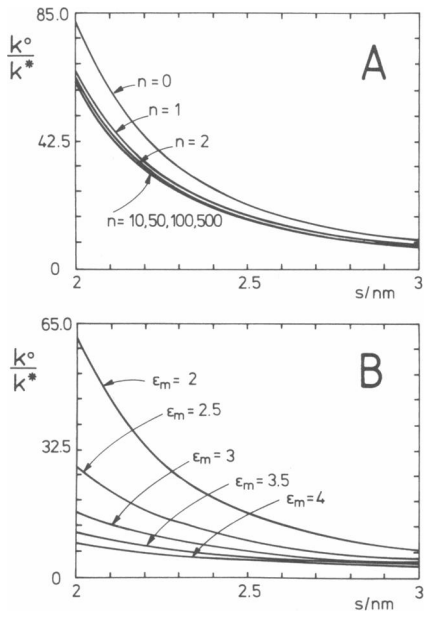

FIGURE 2 (*A*) Fast convergence of the series in Eq. 4 for $\epsilon_m = 2$. The sums were computed for several numbers of terms. It is shown that the sum with $n = 10$ terms has no appreciable difference to that of $n = 500$. In the application of this model the summations were performed up to 100 terms to exclude numerical inaccuracies. (*B*) Electrostatic effects on the rate constants of a charge-translocating reaction step in a protein dimer (Fig. 1). k^0 and k^* are the rate constants under the condition that the charge in the adjacent monomer is still in the original position $x = a$, or has moved to position $x = d - b$, respectively.

Electrostatic coupling in a two-dimensional lattice of pump molecules

As a further system we consider a two-dimensional lattice of pump molecules. Experimental systems to which this treatment can be applied are the purple membrane of halobacteria, as well as membrane preparations containing Na,K-ATPase or Ca-ATPase in high density. In the latter cases, the lattice model would represent an approximation (see Fig. 3 *a*), because the ATPase molecules are usually not ordered in the membrane. In a more realistic model for the nonordered molecules we consider in a subsequent section of this paper the situation in which the pumps are randomly distributed over the nodes of an hexagonal lattice having an average internodal distance equal to the one observed experimentally.

In the following we consider an experiment in which initially the transported ions (H^+, Na^+, Ca^{++}, etc.) are bound to a site within the pump protein. By a fast perturbation such as a light flash or an ATP-concentration jump, a transitory state is created from which release of the bound ions to the aqueous medium on the external side of the membrane may occur (Fig. 3 *b*). We assume that the liganding system in the binding pocket bears a negative charge which electrically neutralizes the charge of the bound ion. Release of bound ions then builds up a time-dependent diffuse space-charge (or Gouy-Chapman) layer on the aqueous side of the external interface (uptake of the ions from the internal solution could also form a Gouy-Chapman layer there, but this layer remains constant during the process of releasing the bound ions). The thickness of the space-charge layer is approximately given by the Debye length l_D:

$$l_D = \frac{1}{F}\sqrt{\frac{\epsilon_0\epsilon_w RT}{2c}}. \qquad (5)$$

F is Faraday's constant and R the gas constant. Eq. 5 holds for the case that the aqueous medium contains a (1:1)-electrolyte of concentration c; in the more general case of a mixture of several ionic species, c has to be replaced by the ionic strength J. In the following electrostatic calculations, the space-charge layer is replaced, as

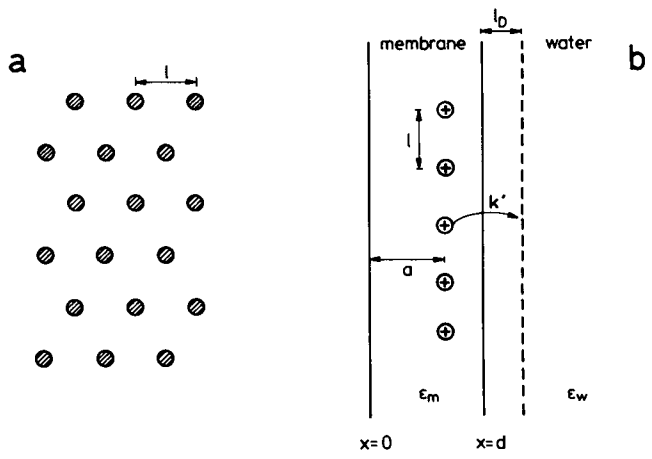

FIGURE 3 (*a*) Frontal view of the hexagonal lattice of membrane-embedded pump molecules. The elemental size is 1. (*b*) Transverse view of the hexagonal lattice of membrane-embedded pump molecules. Upon an initial perturbation of the system bound cations are released from a binding site in the protein. k' is the rate constant of ion release, and l_D is the Debye length in the aqueous phase.

an approximation, by a charged plane located at a distance l_D from the interface (Fig. 3 *b*).

We assume that the pump molecules are arranged in a hexagonal lattice with nearest-neighbor distance l (Fig. 3). The quantity of interest is the rate constant k' of release of the bound ion from a pump molecule in the lattice, which depends on electrostatic interactions with fixed charges and bound ions in the neighboring pump proteins and with charges in the Gouy-Chapman layer. If ion release is initiated by a fast perturbation at time $t = 0$, the rate constant k' will vary with time, as more and more pump proteins in the vicinity of the pump under consideration release a bound ion. At any time t, k' is given by the rate-theory relation:

$$k' = \tilde{k}' \exp\left[Ze_0 \frac{\Psi(a,t) - \Psi(d + l_d, t)}{2k_BT}\right]. \quad (6)$$

Again, Z is the valency of the bound ion. $\Psi(a,t)$ and $\Psi(d + l_D, t)$ are the time-dependent electric potentials at positions $x = a$ and $x = d + l_D$ which are built up by release of ions from the membrane. $\tilde{k}'$ is the rate constant under the initial condition $\Psi(a,t) = \Psi(d + l_D, t) = 0$. (Note that $\Psi(x,t)$ is the change of electric potential resulting from ion release; the influence of a potential difference between $x = a$ and $x = d + l_D$, which may already exist at time $t = 0$ due to the presence of fixed charges, is taken into account by the intrinsic rate constant $\tilde{k}$. This constant also contains the contribution of the Born energy of the ion and all the time-independent external or internal contributions to k', as for example a transmembrane electrical potential.) The fact that Eq. 6 contains the difference $\Psi(a,t) - \Psi(d + l_D, t)$ instead of $\Psi(a,t) - \Psi(d,t)$ corresponds to the notion that the bound ions are released to the bulk solution and therefore have to overcome the total potential difference between binding site and Gouy-Chapman plane.

Simplified treatment: homogeneous distribution of charges

Before we analyze the model of Fig. 3 in a more rigorous way, it seems useful to treat a simplified version of the model from which the order of magnitude of the electrostatic effect on k' can be easily estimated. For this purpose we replace the array of discrete protein charges by a homogeneously charged plane located at $x = a$, and replace (as mentioned above) the diffuse space-charge layer by a homogeneously charged plane located at $x = d + l_D$. In this condition, the potential $\Psi(x)$ varies linearly between $x = a$, $x = d$, and $x = d + l_D$, and remains constant for $x < a$ and $x > d + l_D$. From elementary electrostatic considerations, the time-dependent boundary potential $V_b(t)$ is then obtained as:

$$V_b(t) \equiv \Psi(a,t) - \Psi(d + l_D, t) = -\frac{Ze_0}{\epsilon_0}\left[\frac{d-a}{\epsilon_m} + \frac{l_D}{\epsilon_w}\right] \cdot n(t), \quad (7)$$

where $n(t)$ is the number of protein molecules per unit area that have already released the bound ion.

The maximum value, $n(\infty)$, of $n(t)$ may be taken to be equal to the density of pump molecules in the membrane. With the purple membrane of Halobacterium as an example, $n(\infty)$ is $\sim 70{,}000\ \mu m^{-2}$ (Henderson, 1977). If we consider $Z = 1$, $\epsilon_m = 3$, $\epsilon_w = 80$, $d - a = 1$ nm and $l_D = 1$ nm (corresponding to an ionic strength of ~ 100 mM), the maximum value of V_b, which is reached at long times ($t \to \infty$) after the initial perturbation, becomes $V_b(\infty) \approx -438$ mV. According to Eq. 6, the ratio of the time-dependent rate constants $k'(t)$ at times $t = 0$ and $t \to \infty$ is then given by:

$$\frac{k'(\infty)}{k'(0)} = \exp\left[\frac{Ze_0V_b(\infty)}{2k_BT}\right] \approx 2 \cdot 10^{-4}. \quad (8)$$

This means that the rate constant of ion release strongly decreases during the release process. The time course of the release process may be described by introducing the probability $P(t) = 1 - [n(t)/n(\infty)]$ that a given pump molecule has the ion still bound at time t. $P(t)$ is given by the rate equation:

$$\frac{dP}{dt} = -k'(t) \cdot P. \quad (9)$$

Expressing $k'(t)$ by Eqs. 6 and 7 yields

$$\frac{dP}{dt} = -k'(\infty) \cdot P \cdot \exp(u \cdot P), \qquad (10)$$

where $u = -Ze_0V_b(\infty)/2k_BT > 0$ is a time-independent constant. Eqs. 9 and 10 describe a monomolecular decay process with a time-dependent rate constant. As seen from Fig. 4, the solution for $P(t)$ strongly differs from the single-exponential function $P_e(t)$ which would be predicted for a monomolecular process with a time-independent rate constant $\tilde{k}'$ (here chosen to be $4 \cdot 10^3$). This is evident in the plot of ln $(P(t))$ (*inset*), where a straight line should be expected if $P(t)$ were single-exponential. The spectral analysis of the curve shows that a number of at least 5 exponentials would be necessary to fit it in the given time interval.

Discrete distribution of charges

In the model of Fig. 3 *b*, for $l_D = 0$, we consider that the counter charges also form a discrete distribution on the outer face of the membrane. Then we have two parallel two-dimensional lattices, one inside the membrane formed by the positions of the pumps, and the second in the outer interface formed by the positions of the released ions. At time $t = 0$, both lattices contain no charges and, as the time goes on, ions jump from the internal binding sites of the pumps to the external interface and the released ions leave a negative charge in the lattice of binding sites. In this way the nodes of both lattices become charged up, affecting the potential in the neighboring pumps and altering their rate of transition. For $l_D > 0$ we consider a homogeneously distributed plane in the water solution. This plane becomes charged up as the ions jump into it.

At time t, the potential $\Psi(a, t) - \Psi(d + l_D, t)$ along the axis of one pump is given by the sum of the contributions of all the pumps which have already released the ion. This sum is not a closed-form expression, and it would be too time consuming to evaluate. Therefore, we make the approximation that the charges far away from the pump of interest form a homogeneous distribution. We treat those charges inside a circle of radius H around the given pump as discrete, and the rest are considered as a homogeneous distribution (see Fig. 5). This also corresponds to the notion that the first neighboring pumps give the principal contribution to the time-dependent potential in the pump. The charge density of the homogeneous distribution is taken as proportional to the average number of pumps per unit area which have already released the ion at time t.

Equation 4 gives the potential Ψ inside the membrane when the charge is also inside. Nevertheless, in order to analyze the model in the case for $l_D > 0$ we need to know

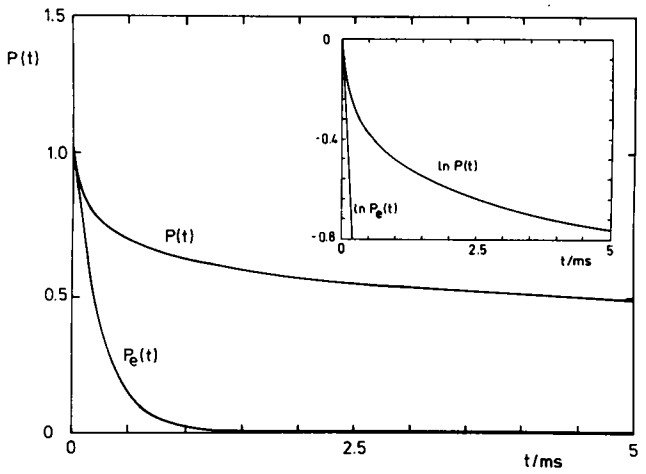

FIGURE 4 Time course of the release of bound ions. $P(t)$ is the probability that a given protein has the ion still bound at time t. The solution of Eq. 10 is compared with the purely exponential decay function $P_e(t) = \exp(-\tilde{k}'t)$, where $\tilde{k}'$ is the intrinsic rate constant for ion release in the absence of potential. Eq. 10 has been numerically evaluated using the following parameter: $Z = 1$, $d - a = 1$ nm, $l_D = 1$ nm, $\epsilon_m = 3$, $\epsilon_w = 80$, $n(\infty) = 70{,}000$ μm^{-2}, and $\tilde{k}' = 4 \cdot 10^4$ s^{-1}. (*Inset*) Natural logarithm of $P(t)$ and $P_e(t)$. Shown are the straight line for ln $(P_e(t))$ with slope $-\tilde{k}$, and the clear nonexponential behavior of $P(t)$.

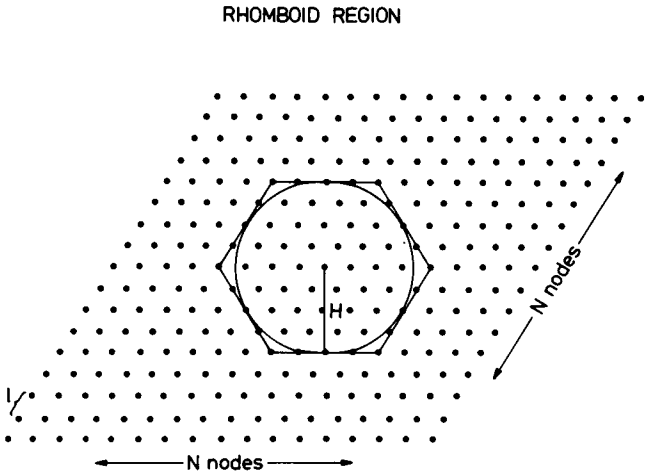

FIGURE 5 Rhomboid region of a hexagonal lattice. The total number of nodes shown is N × N. The nodes outside this region are also considered to form rhomboid regions connected by periodic boundary conditions. The charges inside the circle are considered discrete when calculating the potential $V_b(t)$ along the axis of the central pump. The remaining charges are considered to form a homogeneous distribution. The radius of the circle is $H = (\sqrt{3}/2) \cdot N_H \cdot l$, where $N_H \cdot l$ is the length of one side of the circumscribed hexagon. In order to calculate the contribution of the infinite plane with a circular hole, we subtract the contribution of a disk of radius H from the contribution of an infinite plane without a hole.

the potential in the external region, and we also need it when the charge is outside the membrane. In Appendix A we give the required expressions for the indicated situations.

When the external distribution is considered discrete, the maximum potential $V_b(\infty)$ on the axis of one particular pump, according to the notation used in Appendix A, is given by:

$$V_b(\infty) = Ze_0 \cdot \sum_i [-{}^1\Psi_m(a, l_i) + {}^1\Psi_{we}(d + c, l_i) + {}^2\Psi_m(a, l_i) - {}^2\Psi_{we}(d + c, l_i)], \quad (11)$$

where the sum is extended over all the nodes of the lattice (except the one of the pump of interest), l_i is the distance from the node i to the axis of the pump. Notice that the quantity in brackets is a time-independent function of the magnitudes of the lattice, pumps, membrane, and dielectric constants.

For the given parameters of the purple membrane of halobacterium (with $l_D = 1$ nm), Eq. 11 results in $V_b(\infty) \approx -152$ mV which is ~35% of the homogeneous case (Eq. 7). The difference is due to the fact that the sum in Eq. 11 does not include the contribution of the discrete charges in the pump of interest. These point charges (the binding site and the released ion) would give an infinite contribution to the potential $V_b(\infty)$. On the other hand, for the homogeneous distribution, these charges are taken into account in Eq. 7 in the sense that they are incorporated in the part of the homogeneous layer which are exactly on the binding site and in front of the pump (they are two parallel disks of radius similar to the radius of the pump).

If the distribution inside the membrane is considered discrete and the external as homogeneous, we get for the same parameters the value of $V_b(\infty) \approx -164$ mV. The difference between this value and those from Eqs. 7 and 11 show the magnitude of the contributions from each distribution when considered as discrete or homogeneous.

In the following we describe the two methods used in the calculations of the time evolution of $P(t)$. Then we apply them to a more realistic model of the bacteriorhodopsin pumps. We will see that the values for $V_b(\infty)$ found previously are sufficient for a clear nonexponential behavior of $P(t)$.

1. Mean field approximation

When both distributions of charges are considered discrete, we may use a mean field approximation to describe the time course of $P(t)$. This is done by considering that at time t the average net charge in each pump is:

$$q(t) = Ze_0 n(t)/n(\infty), \quad (12)$$

so that the average potential $\Psi(a, t) - \Psi(d, t)$ on a particular pump is given by:

$$V_b(t) = \Psi(a, t) - \Psi(d, t) = \sum_i \lambda_i q(t) = \left[\frac{Ze_0}{n(\infty)} \sum_i \lambda_i\right] n(t), \quad (13)$$

where i counts for the nodes of the lattice and λ_i is identical with the expression in brackets in Eq. 11. Then, the evolution of the probability $P(t)$ is obtained again from Eqs. 9 and 10 but now the potential $V_b(\infty)$ has the form:

$$V_b(\infty) = Ze_0 \cdot \sum_i \lambda_i. \quad (14)$$

The difference between this $V_b(\infty)$ and the one obtained from Eq. 7, is that Eq. 14 contains the information about the discrete geometry of the system.

2. Stochastic simulation

In the stochastic simulation we perform computer experiments in which we simulate the ion-releasing process of pumps which are distributed over the lattice. In order to explain the way in which this simulation is done, we refer to the model of Figs. 3 *b* and 5.

We take a rhomboid region in the hexagonal lattice with N × N nodes (Fig. 5) and consider periodic boundary conditions. At $t = 0$ all the pumps have an ion bound. At time $t > 0$ some pumps have released the ion and contribute by the charge displacement to the creation of a potential $V_b(t)$ at the place of each pump for which the release has not yet occurred. Now we consider a small increment Δt in time. The time-dependent rate constant $k'(t)$ (which is now different for each pump) is the probability per unit time for the ion to be released at time t. Then, the probability that a given pump releases the ion during the interval Δt is given by $PR = k'(t) \cdot \Delta t$. We generate a random number RN with a homogeneous distribution in the interval (0, 1). If $RN \leq PR$ the pump is allowed to release the ion; if $RN > PR$ the ion remains bound. This is done for each pump in the rhomboid that still has an ion bound. (This procedure is based on the fact that the probability for a random number $r \in (0, 1)$ to be smaller than a given number $x \in (0, 1)$ is equal to x.) Before we consider the next increment Δt in time, the potential is recalculated for each pump which has not yet released the ion. This new potential $V_b(t + \Delta t)$ is the sum of the potential $V_b(t)$ plus the contribution of those pumps which released the ion in the previous step. The process is repeated for each interval Δt into which the whole time interval of observation has been divided.

In this way the ions are released to the external aqueous solution and the potential $V_b(t)$ increases with time in each pump. The quantity of interest in the

process is the transient flux of ions through the membrane. This current is proportional to the time derivative of the probability $P(t)$. This probability is calculated by the number of pumps in the rhomboid which have not released the ion at time t divided by the total number of pumps in it.

In order to calculate the potential $V_b(t)$ on the axis of a given pump, we mentioned above that we sum the discrete contribution of those charged nodes which lie inside a circle of radius H, and the rest is considered as a homogeneous distribution (Fig. 5). The charge density of this homogeneous distribution is taken to be proportional to the total number of ions which have been released from the rhomboid at time t divided by its area. When considering the circle around each pump in the rhomboid, we also incorporate the periodic boundary conditions in the model.

The mean field approximation (MFA) is only an approximation to the real solution given by the stochastic simulation (SS). This point can be illustrated by an exactly solvable model, for example, that of an array of dimers of pumps having a long distance l between them and a short distance s between individual pumps in a dimer (see Fig. 1), so that we only have to consider the electrical interaction inside a dimer as explained earlier. The analytically exact solution is a simple two-exponential decay for $P(t)$. This solution is reproduced by the SS, but not by the MFA. Nevertheless, the MFA is a good approximation for some model parameters (see Appendix B).

We are now prepared to apply the mean field approximation and the stochastic simulation methods to the determination of $P(t)$ to some models of arrays of pump proteins. First we treat the case of ordered arrays like that formed by bacteriorhodopsin, and then, the case of randomly distributed pumps as observed in membrane fragments containing Na,K- and Ca-ATPases.

Ordered distribution of pumps

To use a more detailed model for the bacteriorhodopsin pumps, we take into account that this pump protein appears in trimers in the fragments of purple membrane of halobacteria (Blaurock and Stoeckenius, 1971; Unwin and Henderson, 1975), so that each node in the hexagonal lattice represents three pump proteins, as shown schematically in Fig. 6.

At $t = 0$ all the proteins have bound an H^+ ion within a binding site in the membrane ($P(t) = 1$). Then they start to release them to the external solution. The jumping ions leave charged binding sites, which leads to the described electrical interaction process. The parameters used in the calculations for this model are: $\epsilon_m = 3$, $\epsilon_w = 80$, $d = 5$ nm, $a = 3.5$ nm, $l_D = 0$, $l = 6.3$ nm, $s = 3$ nm, $\tilde{k}' = 4 \cdot 10^4$, $T = 298.5$ K, $\Delta t = 5 \cdot 10^{-6}$, $N_H = 21$, and $N = 200$ (corresponding to 120,000 pumps on the rhomboid). The maximum value of the potential is $V_b(\infty) = -406$ mV. The values for the lattice extension N, the radius H, and the time increment Δt, were chosen appropriately to obtain a smooth curve for $P(t)$ and to reproduce its average behavior with respect to different sequences of random numbers and different total numbers of pumps. The value of the rate constant $\tilde{k}'$ was chosen according to experimentally encountered parameters (Fahr et al., 1981; Holz et al., 1988).

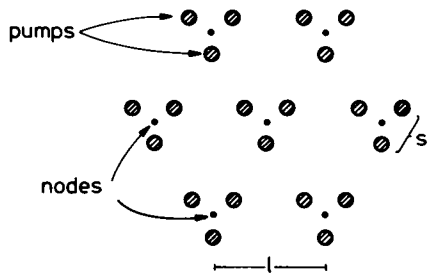

FIGURE 6 Schematic representation of the position in the lattice of the trimers of the pump protein bacteriorhodopsin (Blaurock and Stoeckenius, 1971; Unwin and Henderson, 1975). The values of the distances shown were considered approximately as: $l = 6.3$ nm, and $s = 3.0$ nm.

The results from the mean field approximation and the stochastic simulation are compared in Fig. 7. During the first millisecond the probability $P(t)$ calculated by the SS decays faster than calculated by MFA (not resolved in the plot). They have a crossing point at ~ 1.5 ms, and then the decay of $P(t)$ determined by SS is slower. The difference between the SS and MFA solutions for $P(t)$ as shown in Fig. 7 is similar to the one expected if the trimers were very far from each other, i.e., $l \gg 1$. In the case of independent trimers the model is solvable (analogous to the case of independent dimers treated in Appendix B) and the SS method reproduces the exact solution. Then, for the actual value of l we can estimate the accuracy of the approximation using a MFA.

The main conclusion from Fig. 7 can be seen in the inset. The logarithmic plot of $P(t)$ shows that it is clearly nonexponential. We analyzed the curve corresponding to the SS solution and found that, for the time interval of 15 ms, at least 5 exponentials are required to fit the time course of $P(t)$. Note that, if $l_D > 0$ and/or the external distribution were considered continuous, the maximum potential $V_b(\infty)$ would be increased and, correspondingly, also the nonexponential behavior of $P(t)$.

Random distribution of pumps

An approximate model for the nonordered two-dimensional distributions of pump proteins is made by consid-

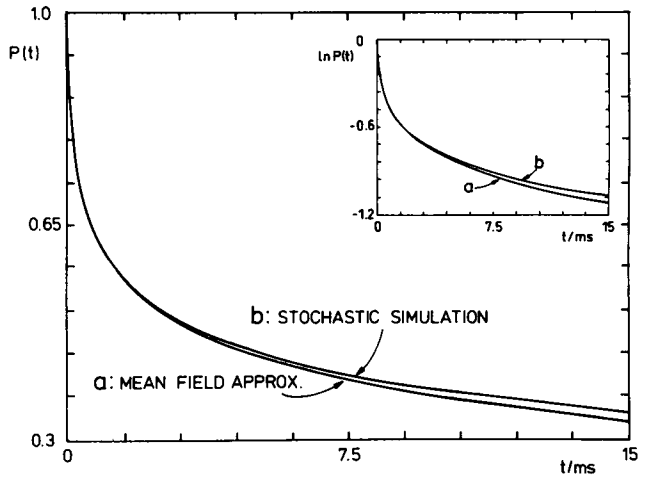

FIGURE 7 Comparison of the solutions for $P(t)$ obtained from the mean field approximation and the stochastic simulation for the hexagonal lattice of trimers of bacteriorhodopsin pump proteins. The parameters used in these calculations were: $\epsilon_m = 3$, $\epsilon_w = 80$, $a = 3.5$ nm, $d = 5$ nm, $l_D = 0$, $l = 6.3$ nm, $s = 3$ nm, $\bar{k}' = 4 \cdot 10^4\ s^{-1}$, $T = 298.5$ K, $\Delta t = 5 \cdot 10^{-6}$ s, $N = 200$ (corresponding to 120,000 pumps on the rhomboid), and $N_H = 21$. The maximum value of the potential is $V_b(\infty) = -407$ mV. (*Inset*) Comparison of the natural logarithm of $P(t)$ from the mean field approximation and the stochastic simulation. Clearly both are nonexponential, and this behavior is more pronounced in the stochastic simulation.

ering an array in which the pumps are randomly located over the nodes of the hexagonal lattice. Here the elemental size of the lattice is the effective diameter of one single pump (or oligomer), and the average distance is in correspondence to the experimentally observed density of pumps. In this situation some nodes are empty, some others have isolated pumps, and there are others forming clusters of two or more pumps.

To apply the SS to this situation we use several random number sequences and take the average behavior for $P(t)$. This average behavior should remain almost invariant when the number of proteins is large enough. For the MFA we consider that each node has, at time t, an average charge $q(t) = Ze_0n(t)/N_P$, where $n(t)$ is the same as before, and N_P is the number density of nodes in the lattice (compare with Eq. 12).

As an example for nonordered distributions of pump proteins purified membrane fragments containing Na,K-ATPase have been chosen, where a density of about 10^4 units per μm^2 has been experimentally found (Deguchi et al., 1977). This density corresponds to an average distance of $\approx$ 10 nm, we consider a model in which the diameter of one unit is $l \approx 6$ nm. (Note that, if they were dimers in place of monomer, the electric interaction effect we are describing would be increased.) The remaining parameters used in this model are: $Z = 1$, $\epsilon_m = 3$, $\epsilon_w = 80$, $d = 10$ nm, $a = 5$ nm, $l_D = 0$, $\bar{k}' = 4 \cdot 10^4$, $T = 298.5$ K, $\Delta t = 7.5 \cdot 10^{-6}$, $N = 200$, and $N_H = 21$. The maximum average value of the potential is $V_b(\infty) = -244.3$ mV, which is the value used in the MFA. (For simplicity only one elementary charge was assumed for the Na,K-ATPase.)

In Fig. 8 the curves IIb and IIc are the probabilities $P(t)$ obtained from the SS and the MFA, respectively, for the presented model. These curves have a crossing point at 1.5 ms. The curve IIa is the SS solution for $P(t)$ when the same proteins are ordered in an hexagonal array having $l = 10$ nm. The maximum potential in this ordered case is $V_b(\infty) = -203.7$ mV. In the time interval of 10 ms the SS solution is fitted with at least 4 exponentials. The difference found between the solutions of the random and ordered distributions shows that the electric interaction is more effective in the random case. This means that, for the nonexponential behavior of $P(t)$, the dominant contribution comes from

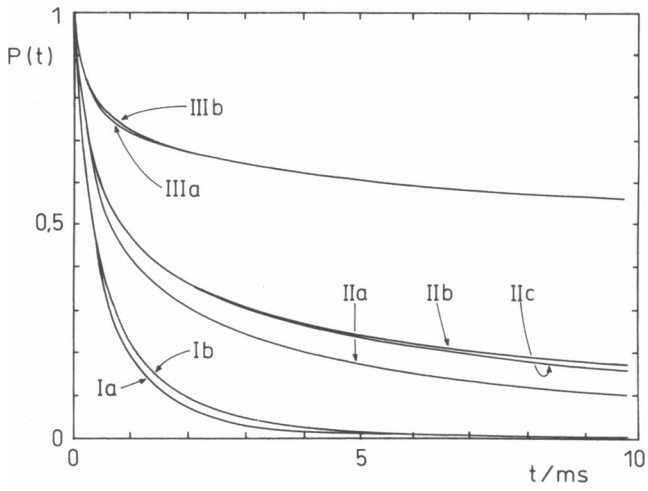

FIGURE 8 Time course of the probability $P(t)$ for the following cases: (Ia) SS for ordered Na,K-pumps (with $a = 2.5$ nm and $d = 5$ nm). (Ib) SS for randomly distributed Na,K-pumps (dimensions as in Ia). (IIa) SS for ordered Na,K-pumps (with $a = 5$ nm and $d = 10$ nm). (IIb) SS for randomly distributed Na,K-pumps (dimensions as in IIa). (IIc) MFA for the Na,K-pumps of IIb. (IIIa) SS for ordered Ca-pumps (with $a = 5$ nm, $d = 10$ nm, $l = 6$ nm). (IIIb) MFA for the Ca-pumps of IIIa. The remaining parameters used in these models are: $\epsilon_m = 3$, $\epsilon_w = 80$, $l_D = 0$, $\bar{k}' = 4 \cdot 10^4\ s^{-1}$, and $T = 298.5$ K. The maximum value of the potential $V_b(\infty)$ is, in each case: (Ia) $V_b(\infty) = -82.4$ mV; (Ib) $V_b(\infty) = -95.2$ mV; (IIa) $V_b(\infty) = -203.7$ mV; (IIb) $V_b(\infty) = -244.3$ mV; (IIc) $V_b(\infty) = -244.3$ mV; (IIIa) $V_b(\infty) = -676.8$ mV; (IIIb) $V_b(\infty) = -676.8$ mV.

those closest proteins in the random array, even when the average distance is the same in both distributions.

Curves IIIa and IIIb in Fig. 8 show the SS and MFA solutions, respectively, for a model of ordered Ca-pumps. In this model we used the same parameters as in the sodium pumps except that the average distance l is ~ 6 nm according to the experimentally found density of $3 \cdot 10^4$ units per μm^2. This average distance is of the order of the pump diameter, and we assume that they are distributed in a hexagonal arrangement. Here the maximum potential is $V_b(\infty) = -676.8$ mV, and it is fitted with at least 4 exponentials in the given time interval. These curves behave like those presented in Fig. AB2.

The curves Ia and Ib in Fig. 8 are the SS solutions for the ordered and random distributions, respectively, corresponding to a model of Na,K-pumps having smaller dimensions: $a = 2.5$ nm and $d = 5$ nm. For this model the maximum potentials are $V_b(\infty) = -82.4$ mV and -95.2 mV, respectively. The corresponding MFA solutions for these parameters are good approximations and coincide almost with these curves (see Fig. AB2 in Appendix B). A minimum number of 4 exponentials is needed to fit the curve Ib in the given interval.

Finally, we have to mention that in the models treated here we considered a charged binding site inside the proteins. Nevertheless, the important factor for the nonexponential behavior of the releasing process is the change in the potential barrier that the jumping ions have to overcome. This change is the same if the binding site is charged or not, and comes entirely from the net displacement of charges in the neighboring proteins. The expressions for calculating this change in the potential barrier are the same in both cases, and we used the assumption of a charged binding site for reasons of clarity in the explanation.

CONCLUSIONS

The electrical interaction between ion translocating pumps in membranes depends mainly on the distance of the charges, the length of the jump, and the dielectric constants of the membrane (Fig. 2 *b*). If the simple case of the release of an ion from a binding site within the protein is analyzed, the deviation of the kinetics from the monomolecular case increases when the distance between the proteins is reduced, as shown in Fig. AB2.

Different approaches have been chosen to calculate the influence of electrostatic coupling of ion pumps: Homogeneous and discrete charge distribution and a mean field approximation and a stochastic simulation. The stochastic simulation gives the real solution of the problem. Differences between mean field approximation and stochastic simulation depend on the set of parameters characterizing the protein system. For some parameters used here, the differences between the two approaches are smaller than typical resolutions of experimental methods.

The time course of the relaxation process determined by stochastic simulation can be fitted by a sum of exponentials. The number of exponentials depends on the model parameters and on the length of the time interval considered. In the cases treated here a number ≥ 4 exponentials was necessary to fit the curves in the given intervals. The findings indicate that, in ion transport processes where this electrical interaction is significant, a correct description should be at least multiexponential for each charge translocating step. An attempt to fit the curves with a continuum distribution of exponentials was not made. Nevertheless, it is clear that, if the real process includes several or more complicated steps, the detailed description would be correspondingly more complicated.

In several tissues ion translocating pumps appear in high densities. Three cases have been investigated and discussed in this paper. In the purple membrane of halobacteria the light driven ion pump bacteriorhodopsin has been found in a crystalline lattice with a lattice constant of ~ 6.3 nm for trimers of the protein and 3 nm distance between single pumps of a trimer (Unwin and Henderson, 1975). In the case of the Ca-pump of the sarcoplasmatic reticulum (SR), where the average pump density is in the order of 30,000 per μm^2, the arrangement of pumps is close to crystalline order (Taylor et al., 1984). The third example discussed is a purified membrane preparation of the Na,K-ATPase, frequently used to determine kinetic properties of this ion pump (Stürmer et al., 1991). This preparation contains protein with a density of 10,000 per μm^2 (Deguchi et al., 1977). In the case of these and other transport proteins with short distances between each other it has to be checked, whether electrostatic coupling occurs.

Consequences may be that intrinsically monomolecular reactions which occur during translocation processes in ion pumps will be modified. These modifications are caused by time dependent electrical potentials, distorting the mono-exponential kinetics without any additional cooperative effects. The apparent result of these electrical interactions is a complex kinetics, as discussed above. This finding can have important consequences in the interpretation of related experimental data.

According to the presented calculations, stronger effects have to be expected for the SR Ca-pump compared with the Na,K-pump (Fig. 8). Experiments have been performed in which the pump density in Na,K-pump containing fragments has been reduced by UV inactivation and the kinetic behavior has been measured at different concentrations of active pumps. Between a fully active preparation and 10% residual activity no significant change in the E1–E2 transition has been detected (W. Stürmer, personal communication). An explanation for the lack of detectable electrostatic coupling cannot be given up to now, because two crucial parameters are only tentatively known: the actual pump density in the preparation and the jump length of charge carrying steps in the pump cycle.

In the case of bacteriorhodopsin there is some discussion about the number and magnitude of the components in the relaxation time spectrum of the proton movement during the pumping process. Commonly it is thought that the relaxation time spectrum of experimentally determined electrogenic signals is directly related to the conformational transitions they perform during the pumping cycle. This is not necessarily true as has been demonstrated in this paper. An additional complication is given by the fact that not only a single reaction step contributes to the observed signal. Holz and coworkers discussed corresponding observations (Holz et al., 1988). They found that the time course of the active charge displacement can be characterized by a continuous relaxation time spectrum. Fits with a sum of exponentials required five to six components and were not well reproducible. They proposed as the origin of this behavior the existence of conformational substates.

APPENDIX A

The potential in a binding site is calculated as a sum of six different contributions produced by: (*a*) discrete binding sites in the membrane and (*b*) in the aqueous phase, plus a homogeneously-charged plane (*c*) within the membrane and (*d*) in the aqueous phase, minus a charged disk of the same charge density as the plane with a radius, *H*, according to the area occupied by the discrete charges (*e*) in the membrane and (*f*) in the aqueous phase. Therefore, we need to know the potential in all the different regions when charges are inside or outside the membrane.

In Fig. A1 a schematic presentation is given for the contribution of a charge (*filled circle*) and its electrical images (*open circles*) when the potential is determined in the membrane (Ψ_m) and in the interior or exterior aqueous phase (Ψ_{wi}, Ψ_{we}, respectively). Membrane thickness is *d*. The origin of the *X*-axes is placed at the left interface of the membrane. Beneath each position of a (image) charge the coefficient used in the summation is given with:

$$\theta = \frac{\epsilon_w - \epsilon_m}{\epsilon_w + \epsilon_m}, \quad \alpha = 1 + \theta, \quad \text{and } \beta = 1 - \theta,$$

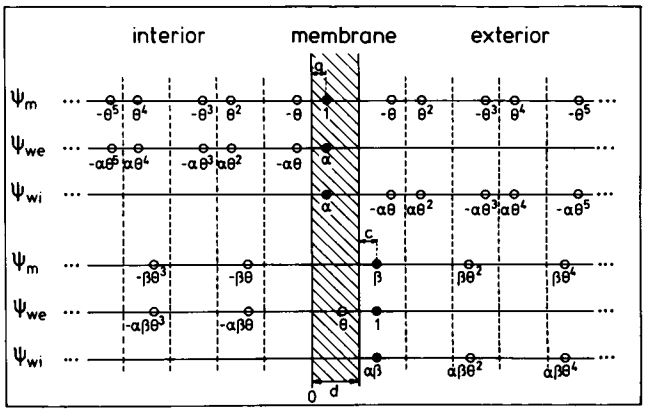

FIGURE A1 Schematic presentation for the contribution of a charge (*filled circles*) and its electrical images (*empty circles*) when the potential is determined in the membrane (Ψ_m) and in the interior or exterior aqueous phase (Ψ_{wi}, Ψ_{we}, respectively). Membrane thickness is *d*. The origin of the *X*-axes is placed at the left interface of the membrane. Beneath each position of a (image) charge the coefficient used in the summation is given with $\theta = (\epsilon_w - \epsilon_m)/(\epsilon_w + \epsilon_m)$, $\alpha = 1 + \theta$, and $\beta = 1 - \theta$. ϵ_m and ϵ_w are the dielectric constants in the water and membrane, respectively.

where ϵ_m and ϵ_w are the dielectric constant in the water and membrane, respectively.

For a unit point charge within the membrane (at $x = a$) the value of the potential at a perpendicular distance l from the *X*-axes is given by (see Eq. 4):

$$
\begin{aligned}
{}^1\Psi_m(x, l) = \frac{1}{4\pi\epsilon_0\epsilon_m}\Bigg[& -\sum_{n=0}^{\infty} \frac{\theta^{2n+1}}{\sqrt{l^2 + (x + a + 2nd)^2}} \\
& + \sum_{n=0}^{\infty} \frac{\theta^{2n}}{\sqrt{l^2 + (x - a + 2nd)^2}} \\
& + \sum_{n=1}^{\infty} \frac{\theta^{2n}}{\sqrt{l^2 + (x - a - 2nd)^2}} \\
& - \sum_{n=1}^{\infty} \frac{\theta^{2n-1}}{\sqrt{l^2 + (x + a - 2nd)^2}}\Bigg]
\end{aligned}
$$

$$
\begin{aligned}
{}^1\Psi_{we}(x, l) = \frac{\alpha}{4\pi\epsilon_0\epsilon_m}\Bigg[& -\sum_{n=0}^{\infty} \frac{\theta^{2n+1}}{\sqrt{l^2 + (x + a + 2nd)^2}} \\
& + \sum_{n=0}^{\infty} \frac{\theta^{2n}}{\sqrt{l^2 + (x - a + 2nd)^2}}\Bigg]
\end{aligned}
$$

$$
\begin{aligned}
{}^1\Psi_{wi}(x, l) = \frac{\alpha}{4\pi\epsilon_0\epsilon_m}\Bigg[& \sum_{n=0}^{\infty} \frac{\theta^{2n}}{\sqrt{l^2 + (x - a - 2nd)^2}} \\
& - \sum_{n=1}^{\infty} \frac{\theta^{2n-1}}{\sqrt{l^2 + (x + a - 2nd)^2}}\Bigg].
\end{aligned}
$$

When the point charge is placed outside the membrane at $x = d + c$, the potential is given by:

$$^2\Psi_m(x, l) = \frac{\beta}{4\pi\epsilon_0\epsilon_m}\left[\sum_{n=0}^{\infty}\frac{\theta^{2n}}{\sqrt{l^2 + (x - c - (2n + 1)d)^2}} - \sum_{n=1}^{\infty}\frac{\theta^{2n-1}}{\sqrt{l^2 + (x + c + (2n - 1)d)^2}}\right]$$

$$^2\Psi_{we}(x, l) = \frac{1}{4\pi\epsilon_0\epsilon_m}\left[\frac{1}{\sqrt{l^2 + (x - c - d)^2}} + \frac{\theta}{\sqrt{l^2 + (x + c - d)^2}} - \alpha\beta\sum_{n=1}^{\infty}\frac{\theta^{2n-1}}{\sqrt{l^2 + (x + c + (2n - 1)d)^2}}\right]$$

$$^2\Psi_{wi}(x, l) = \frac{\alpha\beta}{4\pi\epsilon_0\epsilon_m}\left[\sum_{n=0}^{\infty}\frac{\theta^{2n}}{\sqrt{l^2 + (x + a + (2n + 1)d)^2}}\right].$$

To calculate the potential produced by a disk with radius H and charge density σ in the position $x = a$ or $x = d + c$, respectively, one obtains (with $\phi(y) \equiv \sqrt{y^2 + H^2} - |y|$):

$$^3\Psi_m(x, H) = \frac{\sigma}{2\epsilon_0\epsilon_m}\left[-\sum_{n=0}^{\infty}\theta^{2n+1}\phi(x + a + 2nd) + \sum_{n=0}^{\infty}\theta^{2n}\phi(x - a + 2nd) + \sum_{n=0}^{\infty}\theta^{2n}\phi(x - a - 2nd) - \sum_{n=0}^{\infty}\theta^{2n-1}\phi(x + a - 2nd)\right]$$

$$^3\Psi_{we}(x, H) = \frac{\alpha\sigma}{2\epsilon_0\epsilon_m}\left[-\sum_{n=0}^{\infty}\theta^{2n+1}\phi(x + a + 2nd) + \sum_{n=0}^{\infty}\theta^{2n}\phi(x - a + 2nd)\right]$$

$$^3\Psi_{wi}(x, H) = \frac{\alpha\sigma}{2\epsilon_0\epsilon_m}\left[\sum_{n=0}^{\infty}\theta^{2n}\phi(x - a - 2nd) - \sum_{n=0}^{\infty}\theta^{2n-1}\phi(x + a - 2nd)\right],$$

and

$$^4\Psi_m(x, H) = \frac{\beta\sigma}{2\epsilon_0\epsilon_m}\left[\sum_{n=0}^{\infty}\theta^{2n}\phi(x - c + (2n + 1)d) - \sum_{n=0}^{\infty}\theta^{2n-1}\phi(x - a + (2n - 1)d)\right]$$

$$^4\Psi_{we}(x, H) = \frac{\sigma}{2\epsilon_0\epsilon_m}\left[\phi(x - c - d) + \theta\phi(x + c - d) - \alpha\beta\sum_{n=0}^{\infty}\theta^{2n-1}\phi(x + c + (2n - 1)d)\right]$$

$$^4\Psi_{wi}(x, H) = \frac{\alpha\beta\sigma}{2\epsilon_0\epsilon_m}\left[\sum_{n=0}^{\infty}\theta^{2n}\phi(x - c + (2n + 1)d)\right].$$

The potential produced by an infinite charged plane with charge density σ located at the position of the filled circles in Fig. A1 has the form:

$$^5\Psi_m(x, y) = \gamma_m(y - x) \quad \text{for} \quad a \le x \le y \le d$$
$$^5\Psi_{we}(x, y) = \gamma_w(y - x) \quad \text{for} \quad d \le x \le y$$
$$^5\Psi_{wi}(x, y) = \gamma_w(x - y) \quad \text{for} \quad x \le y \le 0,$$

and

$$^6\Psi_m(x, y) = \gamma_m(x - y) \quad \text{for} \quad 0 \le x \le y \le d$$
$$^6\Psi_{we}(x, y) = \gamma_w(x - y) \quad \text{for} \quad d \le x \le y \le d + c$$
$$^6\Psi_{wi}(x, y) = \gamma_w(x - y) \quad \text{for} \quad x \le y \le 0,$$

with $\gamma_m \equiv \sigma/2\epsilon_0\epsilon_m$ and $\gamma_w \equiv \sigma/2\epsilon_0\epsilon_w$. Here x and y are two points on the X-axes, and $\Psi(x, y)$ is the potential difference $\Psi(x) - \Psi(y)$.

APPENDIX B

When the model is a distribution of dimers which are located very far from each other ($l = \infty$), we have a solvable two-exponential kinetic problem.

One dimer P_1P_2 (see Fig. 1) has four different possible states: (A) P_1P_2, (B) $\overline{P}_1P_2$, (C) $P_1\overline{P}_2$, and (D) $\overline{P}_1\overline{P}_2$, where the bar denotes that the translocation has occurred in the pump. The reaction scheme for the one-way transitions between these four states is:

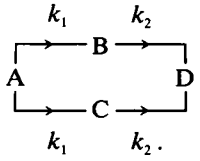

Let $\Pi_i(t)$ denote the probability of the state i (= A, B, C, or D). Because of the symmetry in the rate constants and the initial conditions $\Pi_A(0) = 1$ and $\Pi_B(0) = \Pi_C(0) = \Pi_D(0) = 0$, we have $\Pi_B(t) = \Pi_C(t)$. Then, the kinetic equations are:

$$\frac{d\Pi_A}{dt} = -2k_1\Pi_A, \quad \frac{d\Pi_B}{dt} = k_1\Pi_A - k_2\Pi_B, \quad \text{and} \quad \frac{d\Pi_D}{dt} = 2k_2\Pi_B,$$

with the conservation relation $\Pi_A + 2\Pi_B + \Pi_D = 1$. The solution is:

$$\Pi_A(t) = \exp(-2k_1t),$$

$$\Pi_B(t) = \frac{k_1}{k_2 - 2k_1}(\exp(-2k_1t) - \exp(-k_2t)),$$

and

$$\Pi_D(t) = (1 - \Pi_A(t) - 2\Pi_B(t)).$$

Now, in order to establish the connection to the stochastic simulation, we can say that if the total number of dimers is N, the probability $P(t)$ that a pump has the ion still bound at time t can be written as:

$$P(t) = (2 \cdot N \cdot \Pi_A(t) + N \cdot \Pi_B(t) + N \cdot \Pi_C(t))/(2 \cdot N),$$

or

$$P(t) = \frac{k_2 - k_1}{k_2 - 2k_1} \exp(-2k_1 t) - \frac{k_1}{k_2 - 2k_1} \exp(-k_2 t). \quad \text{(AB1)}$$

(For $k_2 = 2k_1$ the solution can be found from Eq. AB1 in the limit $k_2 \to 2k_1$.)

If the parameters of the dimers, the membrane, and the surrounding medium are: $Z = 1$, s = 2 nm, $a = 4$ nm, $d = 6$ nm, $b = 0$, $l_D = 0$, $\epsilon_m = 3$, and $\epsilon_w = 80$, the potential caused in one pump of the dimer by the other, which has released the ion, is $V_b = -123.9$ mV. Then, given the rate constant k_1, the second rate constant is given by:

$$k_2 = k_1 \exp\left[\frac{Ze_0 V_b}{2k_B T}\right].$$

For $k_1 = 4 \cdot 10^3\ s^{-1}$ and $T = 298.5$ K, we have $k_2 = 3.6 \cdot 10^2\ s^{-1}$.

In Fig. AB1 (case $l = \infty$) the probability $P(t)$ obtained by the exact solution (Eq. AB1) is compared with the stochastic simulation and the mean field approximation. The probability calculated by SS coincides with the exact solution, but there is a large difference compared with the MFA. During the first few milliseconds, the SS probability decays faster than that of the MFA, but then they exchange roles, having a crossing point at ~0.5 ms. This behavior is expected because at the beginning of the releasing process, in the SS method, almost half of the pumps (one in each dimer) have a rate constant k_1 which is conserved for some time. From a certain moment on, almost all the pumps have the rate constant k_2, which is maintained to the end of the process. On the other hand, for the MFA method, the rate constant in each pump decreases continuously from the very beginning, and it has a value which is greater than its minimum value k_2 during the whole time course.

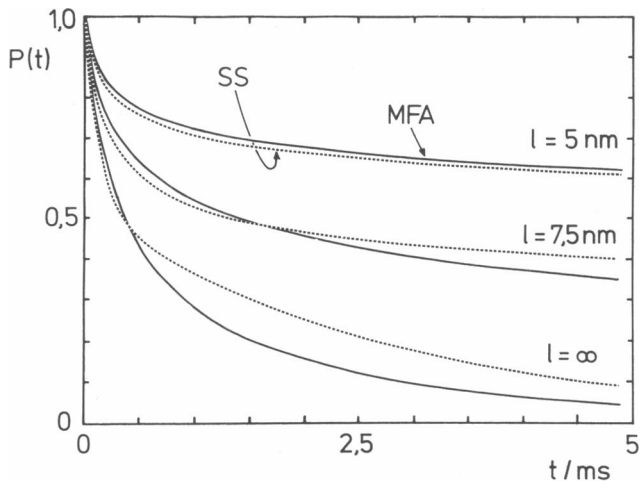

FIGURE AB1 For the model of dimer pumps described in Appendix B (case $l = \infty$), the comparison between the probabilities $P(t)$ obtained by the exact solution (Eq. AB1), the stochastic simulation (*dashed line*), and the mean field approximation (*solid line*) are shown. The exact solution and the stochastic simulation are indistinguishable. In addition the results for this model are presented when the distance l between dimers have the indicated values. We can see how the relation between the SS and MFA solutions is modified by the interaction between dimers. The crossing point for the case $l = 5$ nm occurs at ≈ 15 ms.

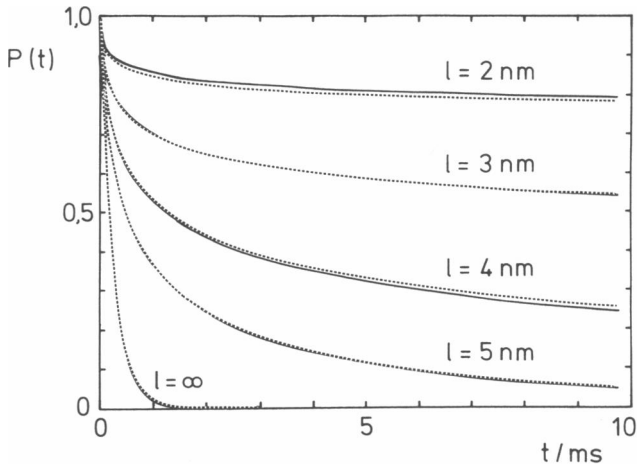

FIGURE AB2 The probabilities $P(t)$ obtained from the stochastic simulation (*dashed line*) and the mean field approximation methods (*solid line*) for an ordered distribution of monomer pumps with dimensions $a = 3.5$ nm, $d = 5$ nm, and the indicated values of l (the remaining parameters are the same as in the model of the Na,K-pumps). The $P(t)$ curves approach the solution of the monomolecular single-exponential reaction when l tends to infinity. The crossing points between the SS and MFA solutions for $l = 5$ nm, 4 nm, and 3 nm, are 1 ms, 1.5 ms, and 7 ms, respectively. For $l = 2$ nm the crossing point is outside the shown time interval.

In Fig. AB1 the solutions for the SS and MFA are shown also when the distance l between dimers have finite values. We can see how the described relation between SS and MFA is modified by the interactions between dimers. The quantitative difference depends also on the other parameters of the model. For the case $l = 5$ nm the crossing point is located outside this time interval, it occurs after about 15 ms. A similar situation is found when we have a distribution of trimers, as in the case of bacteriorhodopsin.

For monomers the relation between the SS and MFA solution is qualitatively the same, but the quantitative difference in the values given by each method is smaller. In Fig. AB2 the SS and MFA solutions are shown for an ordered distribution of single pumps with dimensions $a = 3.5$ nm, $d = 5$ nm, and the indicated values of l (the remaining parameters are the same as in the case of the Na,K-pump). As expected, in distinction to the case of dimers and trimers, the $P(t)$ curves approach the solution of the monomolecular single-exponential reaction when l tends to infinity. The crossing points for $l = 5$ nm, 4 nm, and 3 nm, are at ~ 1 ms, 1.5 ms, and 7 ms, respectively, and for $l = 2$ nm it is outside the given interval. The quantitative differences between the SS and MFA solutions also depend on other parameters of the model, (e.g., the relation between a, d, and l).

This work has been financially supported by the Deutsche Forschungsgemeinschaft (Sonderforschungsbereich 156), and an International Scientific Cooperation fellowship from the Commission of the European Communities to Juan Nieto-Frausto. The cost of the flight Mexico–Germany–Mexico was granted by the Consejo del Sistema Nacional de Educación Tecnológica (convenio 4 J.90).

Received for publication 8 April 1991 and final form 3 September 1991.

REFERENCES

Blaurock, A., and W. Stoecknius. 1971. Structure of the purple membrane. *Nature New Biol.* 233:152–155.

Bühler, R., W. Stürmer, H.-J. Apell, and P. Läuger. 1991. Charge translocation by the Na,K-pump. I. Kinetics of the local field changes studied by time-resolved fluorescence measurements. *J. Membr. Biol.* 121:141–161.

Deguchi, N., P. L. Jørgensen, and A. B. Maunsbach. 1977. Ultrastructure of the sodium pump. Comparison of thin sectioning, negative staining, and freese-fracture of purified, membrane bound (Na^+,K^+)-ATPase. *J. Cell Biol.* 75:619–634.

Fahr, A., P. Läuger, and E. Bamberg. 1981. Photocurrent kinetics of purple-membrane sheets bound to planar bilayer membranes. *J. Membr. Biol.* 60:51–62.

Flewelling, R. F., and W. L. Hubbell. 1986. The membrane dipole potential in a total membrane potential model. *Biophys. J.* 49:541–552.

Gilson, M. K., and B. H. Honig. 1986. The dielectric constant of a folded protein. *Biopolymers.* 25:2097–2119.

Holz, M., M. Lindau, and M. P. Heyn. 1988. Distributed kinetics of the charge movements in bacteriorhodopsin. Evidence of conformational substates. *Biophys. J.* 53:623–633.

Henderson, R. 1977. The purple membrane from halobacterium halobium. *Annu. Rev. Biophys. Bioeng.* 6:87–109.

Honig, B. H., W. L. Hubbell, and R. F. Flewelling. 1986. Electrostatic interactions in membranes and proteins. *Annu. Rev. Biophys. Biophys. Chem.* 15:163–193.

Läuger, P. 1984. Thermodynamics and kinetic properties of electrogenic ion pumps. *Biochim. Biophys. Acta.* 779:307–341.

Läuger, P. 1991. Electrogenic ion pumps. Sinauer Association, Inc., Sunderland, MA. Chapters 8 and 9. 168–251.

Møller, J. V., J. P. Andersen, and M. Le Maire. 1982. The sarcoplasmatic reticulum Ca^{2+}-ATPase. *Mol. Cell. Biochem.* 42:83–107.

Neumcke, B., and P. Läuger. 1969. Nonlinear electrical effects in lipid bilayer membranes. II. Integration of the generalized Nernst–Planck equations. *Biophys. J.* 9:1160–1170.

Nørby, J. G. 1987. Na,K-ATPase: structure and kinetics. Comparison with other ion transport systems. *Chem. Scripta.* 27B:119–129.

Rabon, E. C., and M. A. Reuben. 1990. The mechanism and structure of the gastric H,K-ATPase. *Annu. Rev. Physiol.* 52:321–344.

Stoeckenius, W., and R. A. Bogomolni. 1982. Bacteriorhodopsin and related pigments of halobacteria. *Annu. Rev. Biochem.* 52:587–616.

Stürmer, W., R. Bühler, H.-J. Apell, and P. Läuger. 1991. Charge translocation by the Na,K-pump. II. Ion binding and release at the extracellular face. *J. Membr. Biol.* 121:163–176.

Taylor, K., L. Dux, and A. Martonosi. 1984. Structure of the vanadate-induced crystals of sarcoplasmatic reticulum Ca^{2+}-ATPase. *J. Mol. Biol.* 174:193–204.

Unwin, P. N. T., and R. Henderson. 1975. Molecular structure determination by electronmicroscopy of unstained crystalline specimens. *J. Mol. Biol.* 94:425–440.

Zampighi, G., S. A. Simon, J. Kyte, and M. Kreman. 1986. One-dimensional crystals of (Na^+ + K^+)-ATPase dimers. *Biochim. Biophys. Acta.* 854:45–57.